Evaluating the Critical Thickness of TiO_2 Layer on Insulating Mesoporous Templates for Efficient Current Collection in Dye-Sensitized Solar Cells

Aravind Kumar Chandiran, Pascal Comte, Robin Humphry-Baker, Florian Kessler, Chenyi Yi, Md. Khaja Nazeeruddin, and Michael Grätzel**

In this paper, a way of utilizing thin and conformal overlayer of titanium dioxide on an insulating mesoporous template as a photoanode for dye-sensitized solar cells is presented. Different thicknesses of TiO_2 ranging from 1 to 15 nm are deposited on the surface of the template by atomic layer deposition. This systematic study helps unraveling the minimum critical thickness of the TiO_2 overlayer required to transport the photogenerated electrons efficiently. A merely 6-nm-thick TiO_2 film on a 3-μm mesoporous insulating substrate is shown to transport 8 mA/cm^2 of photocurrent density along with ≈900 mV of open-circuit potential when using our standard donor-π-acceptor sensitizer and Co(bipyridine) redox mediator.

1. Introduction

Since the successful implementation of the titanium dioxide in the field of photocatalysis during early 1970s,[1] the material has become one of the favored oxides in many energy related applications including dye-sensitized solar cells (DSC),[2–5] quantum dot sensitized solar cells,[6] polymer photovoltaics,[7] and water splitting.[8] The primary interest in the material is driven by the scientific significance of its electronic properties and the ease of nano-structuring by variety of synthetic procedures apart from its non-toxicity, chemical stability and the availability.[9] In DSC, the nanoparticle TiO_2 photoanode provides very high surface area for enhanced sensitizer uptake ensuring better light harvesting efficiency and it is coupled with a redox electrolyte and a Pt-coated TCO counter electrode, to complete the cell architecture. Following the photon absorption, the excited electron (e^-_{cb}) in the sensitizer molecule is injected into the TiO_2 conduction band and the oxidized dye is regenerated by the redox mediator or hole conductor adjacent to it. Finally the circuit of electron flow is completed by electron transport from TiO_2 through the external circuit, and the counter electrode back to the electrolyte generating the photocurrent. The mesoporous TiO_2 is an integral part of the system as it supports the dye molecules, transport the injected electrons to the external contact and allows the shuttling of ox/red species within the mesoporous layer during dye regeneration process.[2–5,10] Since the advent of DSC technology, TiO_2 has been exploited in several morphologies like nanoparticles,[11] nanotubes,[12] nanowires,[13] and nanotrees[14] to enhance the charge transport rate and/or the light confinement. However, mesoporous nanoparticle (np) films dominate the photovoltaic performance as they exhibit a better balance between the dye uptake, optical transparency and the carrier transport. In this work, we developed a photoanode which consists of a conformal layer of titanium dioxide (thickness between 1 and 15 nm) on a screen printed mesoporous np-SiO_2 template. The schematic diagram of the photoanode is shown in **Figure 1**A. The TiO_2-on-(np-SiO_2-template) keeps intact the aforementioned properties of the nanoparticles and simultaneously benefiting the templated photoanode concept. The atomic layer deposition (ALD) technique is employed in this study for the deposition of titania due to its ability to form conformal coatings on the high aspect ratio structures by the surface saturative and self-limiting growth process.[15,16] The conformal ALD TiO_2 film on the SiO_2 results in relatively low electronic defects that otherwise can have a significant presence at the interface of the nanoparticles after the sintering process at 500 °C.[17] Also, the use of thin TiO_2 films reduces the chemical capacitance of the oxide which scales with its volume. This in turn will cut down the photovoltage losses due to the capacitive charging. The photovoltaic properties of these modified electrodes are investigated in a DSC using an organic donor-π-acceptor dye (coded Y123, Figure 1B) and Co(bipyridine) redox mediator. Previously, a study has been carried out on a highly porous (>90%), soft and fragile 25 μm film of SiO_2 aerogel framework synthesized under cryogenic temperatures and exploiting the material as a photoanode for DSC.[18] As the film thickness (25 μm) exceeds the diffusion length (L_n) of the conduction band electrons (e^-_{cb}), the collection of the carriers from the far end of transparent conducting glass (TCO) is incomplete

A. K. Chandiran, P. Comte, Dr. R. Humphry-Baker, Dr. F. Kessler,[+] Dr. C. Yi, Dr. M. K. Nazeeruddin, Prof. M. Grätzel
Laboratory of Photonics and Interfaces
Institute of Chemical Sciences and Engineering
Swiss Federal Institute of Technology (EPFL)
Station 6, 1015 Lausanne, Switzerland
E-mail: mdkhaja.nazeeruddin@epfl.ch; michael.graetzel@epfl.ch
[+] Present address: Siemens AG, Corporate Technology, CT RTC MAT MPV, Günther-Scharowsky Strasse 1, D-91058 Erlangen, Germany

DOI: 10.1002/adfm.201202956

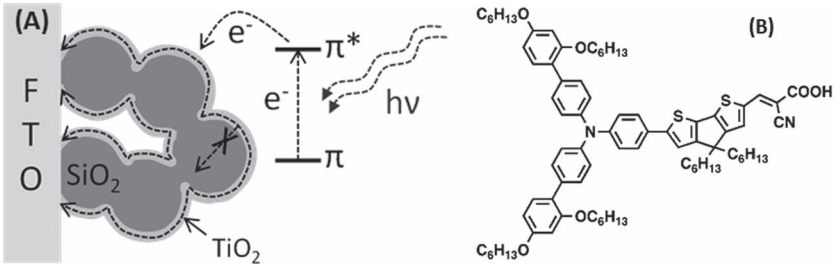

Figure 1. A) Schematic diagram of the TiO_2 deposited on mesoporous nanoparticle SiO_2 template sensitized with the dye. B) Chemical structure of the organic donor-π-acceptor sensitizer coded Y123.

due to loss by recombination process.[19] This poses a restriction on the identification of critical thickness (t_c) of the electronically active TiO_2 overlayer required for efficient carrier transport in the templated structures. Hence in this study we employed only 3 µm mesoporous screen printed SiO_2 film with a nominal surface area of 90 m^2/g and a porosity of 80%. The thickness of silica layer is much less than the L_n of e^-_{cb} and hence the transport limitation has to arise from the overlayer thickness (on SiO_2) and their electronic properties. Our findings show that the t_c of TiO_2 required for the efficient current collection on a 3 µm mesoporous film is only 6–8 nm. Besides the fundamental understanding of electron transport, this study shows significant saving in the TiO_2 utilization on the SiO_2 substrate which can decrease the overall material cost for DSC fabrication. The ability of the electron percolation along the grain boundary free ALD TiO_2 and our conventional np-TiO_2 is compared. Finally we generalize the concept of templates by verifying the photovoltaic properties of the TiO_2 overlayer on other insulating substrates like ZrO_2 and Al_2O_3.

2. Results and Discussion

The amorphous SiO_2 mesoporous film used in this study has a particle size, pore diameter (P_D) and porosity of 28 nm, 60 nm, and 80%, respectively. The films with pore diameter of 60 nm are selected to ensure uniform deposition and avoid diffusion limitation of the metal precursors during TiO_2 deposition. While depositing x nm TiO_2, the pore diameter will decrease to 60–2× and the available P_D for the very next cycle of deposition is reduced from 60 to 60–2× which is still sufficient for precursor diffusion. Our previous study, that involves the deposition of the Ga_2O_3 tunneling layer on mesoporous titania, shows good quality deposition with a P_D of 30–32 nm.[20] The bigger pore of the initial silica template also helped us investigating range of TiO_2 overlayer thickness (1 nm to 15 nm) without narrowing down the P_D to lower values that will lead to the limitations for transport of redox species in DSC under operation.[21,22] The thickness of the ALD layer is measured by depositing similar layers on a Si wafer using spectroscopic ellipsometry (Supporting Information Figure S1). The growth of the titania on Si is linear with the number of cycles and the growth rate is found to be ~0.066 nm/cycle, that is, roughly 15 cycles of deposition gives 1 nm TiO_2. The growth of TiO_2 on Si wafer proceeds from the native silicon oxide layer and so the growth phenomenon is expected to be similar on the nanoparticle mesoporous SiO_2 template.

The crystal structure of TiO_2 deposited on the mesoporous silica, after sintering at 500 °C, is analyzed using X-ray diffraction. When the TiO_2 film thicknesses are ≥ 8 nm (**Figure 2**(c–f)), several reflections are observed over the range of 20° to 80° Bragg angle (2Θ) and can be attributed to the tetragonal lattice crystallized in anatase structure with a space group symmetry of $I4_1/amd$. When the deposited film thicknesses are 5 and 3 nm (Figure 2(a,b)), only one peak at ~25.3° is observed and by following the trend of thicker films, this reflection can be intuitively ascertained to the diffraction of the incident X-ray beam from anatase (101) crystal plane. The broad peak between 20° and 35° comes from the amorphous SiO_2 mesoporous template. With the Fullprof software, the diffractograms are refined to extract the lattice parameters of the ALD titania films ≥8 nm. The values for *a* and *c* are found to be around 3.7865 and 9.5040 Å with estimated error values of ±0.0015 and ±0.0020, respectively. The cell parameters obtained for the ALD films are similar to standard TiO_2 nanoparticles synthesized in our laboratory that are used for high efficiency DSC.[23,24] The above result suggests that the deposition on the amorphous silicon oxide substrate does not significantly influence the intrinsic crystal structure of the TiO_2 film. Following the crystal structure, the chemical state of the film is analyzed using X-ray photoelectron spectroscopy (XPS). The titanium ion in the ALD film, after sintering at 500 °C, exhibit binding energy peaks at ~458.5 eV (Ti $2p_{3/2}$) and 464.4 eV(Ti $2p_{1/2}$) which shows the presence of Ti in +4 oxidation state (Supporting Information Figure S2A).[25] Even though the XPS study is done on the TiO_2 (10 nm) deposited on the SiO_2 mesoporous film, no signal corresponding to Si is observed and it eases elemental analysis by eliminating the

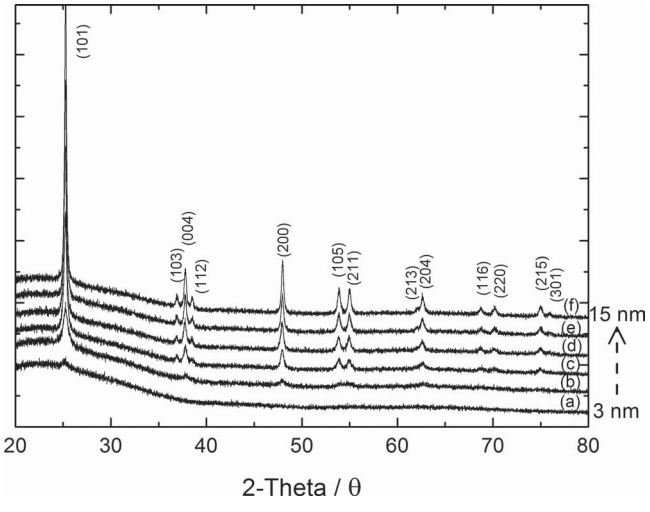

Figure 2. X-ray diffractograms of different thickness ((a) 3 nm, (b) 5 nm, (c) 8 nm, (d) 10 nm, (e) 12 nm, (f) 15 nm) of titania deposited on SiO_2 substrate, after sintering at 500 °C. The reflections are marked with the corresponding (*hkl*) planes.

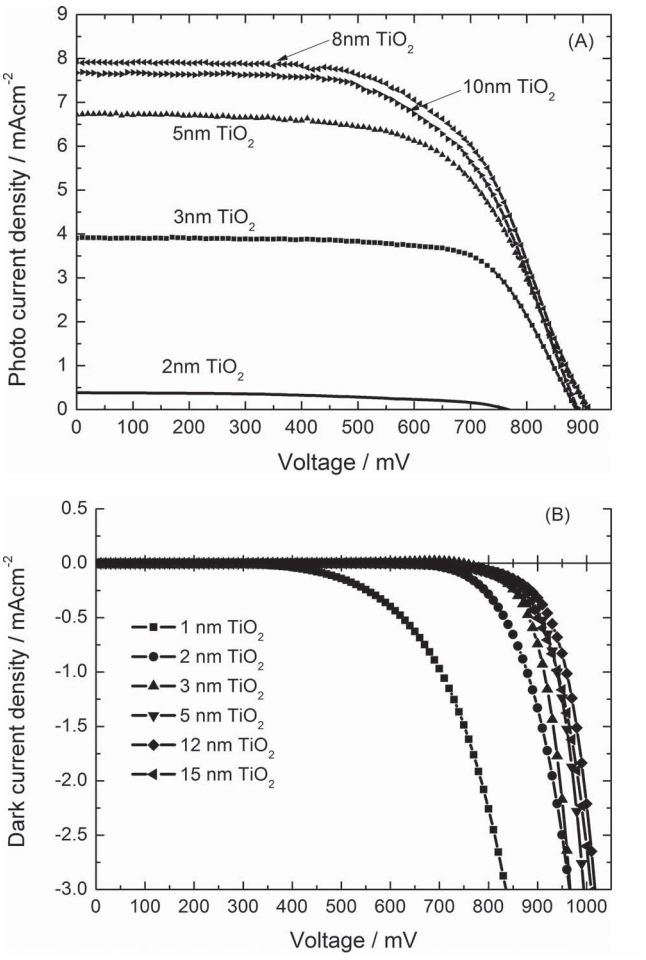

Figure 3. The current-voltage characteristics measured under A) AM 1.5 G solar irradiance (100 mW/cm^2 photon flux); B) dark, for solar cells with different thicknesses of titania on SiO_2 template.

Table 1. The photovoltaic characteristics of the dye-sensitized solar cells are given for different thickness of the titanium dioxide deposited on the silica mesoporous template.

Thickness of TiO_2 [nm]	J_{SC} [mAcm^{-2}]	V_{OC} [mV]	FF [%]	Power conversion efficiency [%]
1	0.1	385.9	35.0	0.02
2	0.4	766.6	48.2	0.14
3	4.0	887.8	70.8	2.5
4	3.8	881.7	66.2	2.3
5	6.9	907.4	61.8	3.9
6	7.9	912.4	57.8	4.2
8	8.2	912.9	59.4	4.4
10	7.8	891.3	59.8	4.2
12	7.7	920.3	56.7	4.0
15	7.3	903.2	55.4	3.7

oxygen contribution from silica. The overlayer is stoichiometric and it exhibits the chemical formula of TiO_2 after the deconvolution of oxygen contribution from hydroxyl group (dark cyan solid line in Supporting Information Figure S2B), H_2O or adsorbed oxygen (blue solid line in Supporting Information Figure S2B).[26] The spectra devoid of Si signal indicate the presence of a crack free, continuous and non-disruptive TiO_2 phase over the template.

To evaluate the efficacy of these electrodes in dye-sensitized solar cells, devices are made using our standard high molar extinction coefficient organic D-π-A sensitizer (48 000 M^{-1}cm^{-1}) and Co(bipyridine) redox mediator (0.56 V vs. NHE).[21] The photovoltaic characteristics of the devices are analyzed under AM 1.5G solar irradiation (100 mW/cm^2 photon flux). The DSC with smaller than 2 nm TiO_2 delivered a photocurrent density (J_{SC}) of less than 0.5 mA/cm^2. An increase to 3–4 nm, enhanced the J_{SC} significantly to around 4 mA/cm^2 reaching to a maximum of ca. 8 mA/cm^2 for 6–8 nm overlayer. The increase of layer thickness beyond 8 nm results in a drop of J_{SC}. The *J–V* curves are shown in **Figure 3**A and the data are presented in **Table 1**. The photocurrent density obtained with *J–V* measurements match closely with the integrated current under the incident-photon-to-electron conversion efficiency (IPCE) spectrum of the corresponding devices. The IPCE could not be measured accurately for the cells with 1 and 2 nm TiO_2 due to the low photo-current levels and so the spectra are not included in the plot (**Figure 4**).

Similarly to J_{SC}, an increasing trend in the open-circuit potential of the devices is observed. The DSC with 1 nm TiO_2 exhibits a very low V_{OC} of ~390 mV and it increased already to ~770 mV for 2 nm. The solar cells containing an overlayer of 3 nm displays a V_{OC} of ~900 mV and remains constant with further increase in the thickness. The evolution of V_{OC} can be explained by measuring the *J–V* profile of similar devices in dark and Figure 3B shows the dark current-voltage plot. The dark current onset starts at 350 mV when the thickness of the layer is 1 nm while further increase to 2 nm shifts the onset to ~700 mV. Beyond 3 nm the dark current profile remains almost

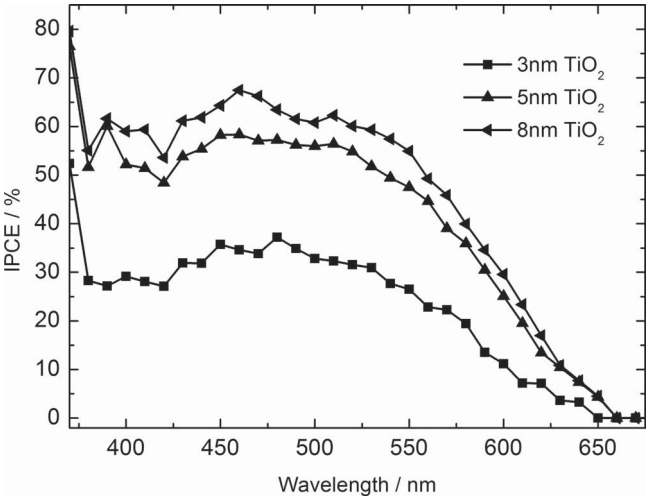

Figure 4. The incident-photon-to-electron conversion efficiency of DSC with photoanodes possessing different layers of TiO_2 on insulating mesoporous template.

similar and the onset is found between 750 and 800 mV. The dark current originates from the recombination of photogenerated electrons at FTO-electrolyte and TiO_2-electrolyte interface, on forward biasing. The recombination of electrons from FTO is shown to be significantly higher than at TiO_2 with cobalt redox shuttle and so very thick under layer of TiO_2 or as shown in ref.[20] insulating layers like Ga_2O_3 have to be used. One has to note that the deposition of TiO_2 on the silica template also covers the conducting substrate of the photoanode. In this study, when the thickness of the layer is 1 or 2 nm TiO_2, the recombination at the FTO-electrolyte interface dominates resulting in the low open-circuit potential. However, when the thickness increases to 3 nm or above, the back reaction is significantly reduced as seen from the dark current onset and hence the V_{OC} remains constant. We exclude the effect of recombination from the SiO_2-electrolyte interface as SiO_2 is completely covered by titanium oxide and also the applied potential (0–0.8 V) is not enough to extract electrons from SiO_2 to induce a redox reaction at its interface with electrolyte.

To rationalize the evolution of the photocurrent, studies on dye uptake, distribution of surface electronic defect states and transport rate are carried out. The amount of dye loading on the surface of the 3 μm silica film is measured by absorption spectroscopy and the variation of dye uptake is monitored by the change in the absorbance maximum at 462 nm. The absorbance change is plotted as the function of the thickness of the titanium dioxide overlayer and is displayed in Supporting Information Figure S3. The SiO_2 reference film adsorbs negligible amount of dye molecules onto its surface and when the TiO_2 is deposited, the absorbance change is significant and rises steadily until 4 nm and then started to decrease slowly. The increase in the dye content until 4 nm might be attributed to the pH of the adsorbing surface while the decrease later (beyond 4 nm) can be explained by the reduction in the internal available surface area due to the deposition of TiO_2 as illustrated in the Supporting Information Figure S3.[27]

The variation in the thickness of the titanium dioxide has an influence on the surface electronic properties, particularly, the distribution of density of trap states (DOS) present below the conduction band of the titanium dioxide due to unsaturated bonds at the termination of crystals and bulk defects.[28] The DOS can be calculated directly by measuring the capacitance of the film using the following equation

$$\mathrm{DOS} = (6.24 \times 10^{18})\mathrm{C}/[\mathrm{d}(1 - \mathrm{p})] \quad (1)$$

where C is the capacitance, d is the thickness of mesoporous film and p is the porosity of the photoanode film.[29] Similar to the nanoparticle titanium dioxide, the surface trap states distribution for ALD TiO_2 overlayer film exhibits an exponential increase when moving towards the conduction band.[10,19] From **Figure 5**, one can note that at any given voltage the density of the trap states is higher for the thinner ALD layers (<5 nm). Beyond 6 nm thicknesses of TiO_2, the amount of electronic trap levels remains constant. This result illustrates that the thinner layers have more defects (until 5 nm) than the thicker layers (≥6 nm) Similar to the IPCE, the photocurrent transients for devices with 1 and 2 nm TiO_2 could not be measured as it involves very low transient currents.

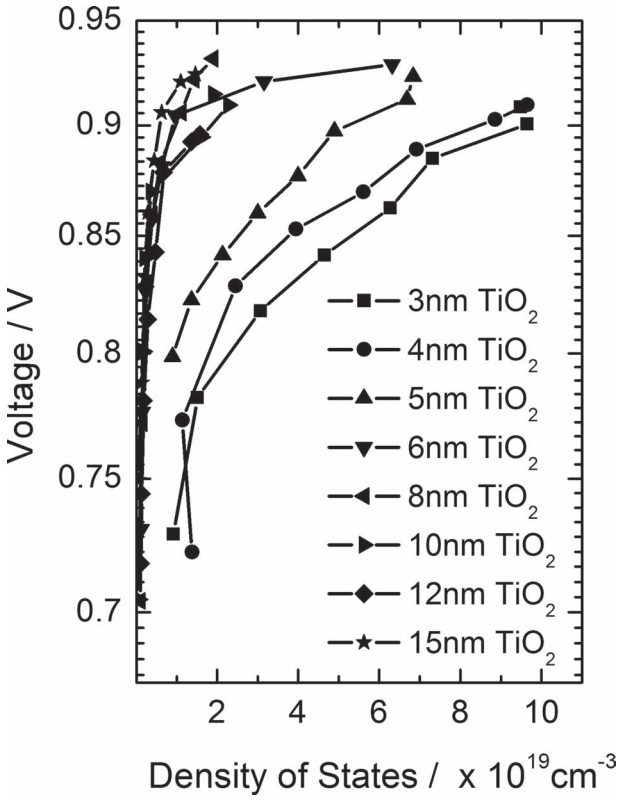

Figure 5. Plot of the evolution of density of trap electronic states (directly proportional to the capacitance, see text for more details) present below the conduction band, for different thicknesses of ALD titanium dioxide.

The variation in the electronic properties of the titania film also has an influence on the transport of the photogenerated carriers. **Figure 6** shows the evolution of the transport rate of electrons measured by photocurrent transient decay technique plotted as a function of the charge density. At a charge density of 10^{19} #/cm^3, a 3 nm TiO_2 overlayer has a transport rate (τ_{trans})

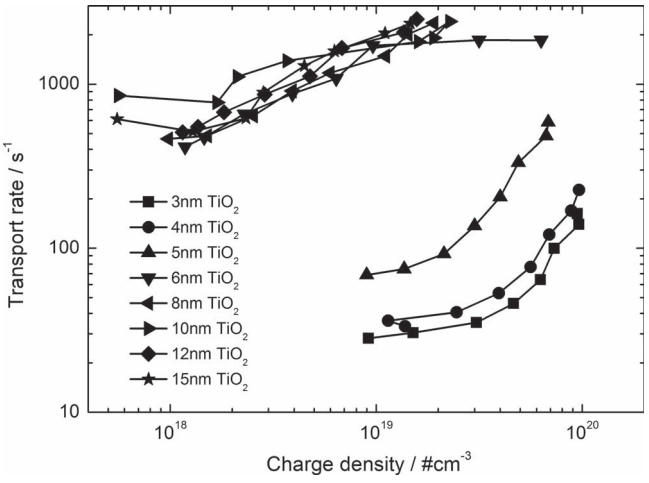

Figure 6. Transport rate (k_{trans}) of the photogenerated electrons plotted as a function of charge carrier density for solar cells with TiO_2 thickness between 3 and 15 nm.

of ~30 s^{-1} followed by a slow increase until 5 nm, while the devices with 6 nm thick ALD titania exhibited sudden increase of τ_{trans} by more than an order of magnitude. The atomic layer deposition of titanium dioxide films thicker than 6 nm did not significantly affect the transport properties of the photogenerated charge carriers. The evolution of τ_{trans} can be explained based on the electronic density of states (Figure 5) and/or the crystallinity of the films. Our previous study on the Nb doping in TiO_2 revealed the sluggish transport of electrons due to the presence of the deeper trap states.[23] The deeper the distribution of electronic defect levels, the more time it takes for the trapped electrons to thermally liberate back to the conduction band of the semiconductor and as a consequence the mobility of the carrier is decreased. In the present case, the SiO_2 mesoporous film with 3–5 nm TiO_2 overlayer also exhibited deeper trap states and hence the transport is lowered. Another probable reason for the slow transport in this regime can be the presence of discontinuities and/or non-crystalline domains that might disrupt the current collection. For the TiO_2 layers greater than or equal to 6 nm, the distribution of trap electronic levels are shallow and similar and hence no change in the mobility is expected. So the similarity in transport properties is strongly supported by the trap state distribution.[19] We also compared the transport rate of the best performing 8 nm ALD TiO_2 on SiO_2 with our standard mesoporous 20 nm titanium oxide nanoparticle film used in conventional dye-sensitized solar cell. From Supporting Information Figure S4 it can be seen that the transport of the charge carriers is faster in the ALD TiO_2 layer compared to the np-TiO_2. This is due to the fact that ALD layer is conformal with less number of defects whereas at every interface of the conventional np-TiO_2, the electronic states are distorted compared to the bulk. This distortion in the electronic band hampers the electron transport between nanoparticles. However ALD TiO_2 does not have many grain boundaries as it is just a conformal film on the SiO_2 and so the percolation of photogenerated carriers is extremely fast. The collection efficiency (η_{coll}) of the device is calculated from the ratio of the transport rate to the sum of transport and recombination rate (Supporting Information Figure S5). Supporting Information Figure S6 shows the plot of the collection efficiency as a function of charge density for various TiO_2 thicknesses. The η_{coll} is found to be higher for the thicker TiO_2 than the thinner ones, which is consistent with the observed photo current density.

Based on the discussions made we classify the evolution of the short-circuit current density into three regimes (Supporting Information Figure S7). *Region 1*- Devices with 1 and 2 nm TiO_2: The low J_{SC} in this region can come from the limitations of electron transport due to the low layer thickness, low dye uptake and possibly due to the discontinuity in the film. *Region 2*–Devices with 3 to 5 nm overlayer: In this region J_{SC} variation is attributed purely to the transport limitation due to the deeper trap states. As shown previously, the dye uptake is not affected in this region. *Regions 3*–Devices ≥ 6 nm overlayer: the current density in this region appeared to be the maximum and is consistent with the observed transport rate. The decrease in the J_{SC} beyond 8 nm arises from the lowering of the dye uptake.

Finally to verify the utility of ALD overlayers on other insulating templates, we investigated the photovoltaic performance of solar cells by depositing TiO_2 on a 3 μm ZrO_2 and Al_2O_3 mesoporous substrates. For this study, we employed an organic dye (Figure 1B) and a Ru (II) metal complex sensitizer (Supporting Information Figure S8) with our standard triiodide/iodide redox mediator. Due to the smaller pore diameters of the mesoporous ZrO_2 and Al_2O_3 films, the thickness of TiO_2 ALD layers were limited to less than 5 nm and 3 nm, respectively. Our efforts in thicker deposition resulted in the clogging of pores. From the *J–V* data presented in Supporting Information Table S1 (ZrO_2) and S2 (Al_2O_3), we see that the trend of photovoltaic performances are similar to that observed with SiO_2. So, it can be generalized that the titanium dioxide overlayer can function as an efficient charge transporter irrespective of the insulating substrates, dyes or redox mediators used to construct DSC. The *J–V* curves for the corresponding best ZrO_2 and Al_2O_3 templated solar cells are presented in Supporting Information Figure S9 and S10.

3. Conclusions

In summary, we introduce the concept of the templated photoanode on the mesoporous insulating oxide by preserving the high surface area of the nanoparticles. This work also unravels the minimum critical thickness (6–8 nm) of titania overlayer for the efficient transport of electrons in the dye-sensitized solar cells. In addition, we show that the transport of electrons in the ALD deposited conformal TiO_2 layer is substantially faster than in the conventional np-TiO_2 films. We also confirmed the general validity of the concept by testing similar layers with different insulating mesoporous templates (ZrO_2 and Al_2O_3), dyes (Y123 and C106) and redox mediator (I_3^-/I^-). Further study will aim at the use of cheap insulating substrates like SiO_2 with optimized mesoporous properties to have a better balance between the deposition conditions and the available surface area for dye uptake. This is expected to pave the road to high efficiency dye-sensitized solar cells. Apart from the scientific advantages, this work highlights the reduction in the material usage. Instead of pure titanium dioxide film as photoanode for DSC using a 6–8 nm ALD titania saves the amount of TiO_2 significantly. An extension of this work with doped TiO_2 can be performed to further improve the charge collection efficiency as shown previously in the literature.[23,24]

4. Experimental Section

Photoanode Preparation: All the solvents and reagents used in this study are of puriss grade. Unless otherwise mentioned, the materials are used as received without further purification. The hydrophilic fumed SiO_2 (aerosol 90, Evonik Industrie AG, Germany) is made into a screen printable paste using ethyl cellulose of two different viscosities and terpineol, following the procedure similar to the TiO_2 paste preparation described in literature.[23]. The mean particle size was 28 nm with a pore diameter and porosity of 60 nm and 80%, respectively. The paste was screen printed onto a pre-cleaned TCO glass (NSG 10, Nippon sheet glass, Japan) followed by a series of sintering steps (125 °C for 10 min with ramp time 5 min, 325 °C for 5 min with 15 min ramp time, 375 °C for 5 min with 5 min ramp time, 450 °C for 15 min with 5 min ramp time and 500 °C for 15 min with 5 min ramp time) and the sintered films was used for the deposition of TiO_2 by ALD. The thickness of the printed film

after sintering was measured using a KLA Tencor alpha-step 500 surface profilometer and was found to be 3.0 ± 0.1 µm.

ALD of TiO_2: The deposition of titanium dioxide on the screen printed mesoporous silicon oxide template is achieved using atomic layer deposition (ALD) instrument (Cambridge Nanotech Savannah S100 apparatus).[20] The deposition was carried out using successive pulses of tetrakis(dimethyl amido)titanium (TDMAT, Aldrich, Germany, 75 °C) and deionized water (18.2 MΩ, 25 °C) using nitrogen as a carrier gas (5 sccm). Following the 100 ms TDMAT or 10 ms H_2O pulse, the precursors are confined inside the ALD reactor for 30 s (exposure time) to ensure a complete exposure inside the mesopores of photoanode. Up to 300 cycles of deposition were carried out on SiO_2 substrates and used as photoanodes for DSC after sintering at 500 °C before dipping the electrodes in the dye solution.

Material Characterization: For the identification of thickness of ALD titania layer, similar number of cycles with identical growth conditions were deposited on Si wafers and measured using spectroscopic ellipsometer with photon energies over the range of 1 to 6 eV (Sopra GES 5E). The obtained spectra were fitted using modified-Cauchy dispersion law to extract the thickness of the deposited TiO_2 layers. The crystallographic properties of the TiO_2 deposited on mesoporous SiO_2 were studied by X-ray diffraction with Bruker D8 Discover apparatus. The diffractograms are refined using Fullprof software following the procedure described elsewhere to extract the lattice cell parameters.[23] The chemical properties of the deposited TiO_2 photoanodes on silica template were probed using X-ray photoelectron spectrometer (XPS/ESCA KRATOS AXIS ULTRA) with Al Kα X-ray radiation of 1486.7 eV. The elemental quantification is obtained by fitting the titanium and the oxygen spectra using CasaXPS (version 2.3.15) software after the subtraction of the background with Shirley model. The dye loading on different samples are measured by desorbing the adsorbed dye in DMF containing basic salt using Cary 5 UV-visible-NIR spectrophotometer (Australia).

DSC Assembly: The synthetic procedures for the Y123 dye (3-{6-{4-[bis(2′,4′-dihexyloxybiphenyl-4-yl)amino-]phenyl}-4,4-dihexyl-cyclopenta-[2,1-b:3,4-b′]dithiphene-2-yl}-2-cyanoacrylic acid) (Figure 1B) and $[Co^{II}(bpy)_3](PF_6)_2/[Co^{III}(bpy)_3](PF_6)_3$ (redox potential = 0.56 V *vs* NHE) are described elsewhere.[30] The ALD TiO_2 overlayer of different thicknesses (1, 2, 3, 4, 5, 6, 8, 10, 12, and 15 nm) on mesoporous SiO_2 substrate were sintered at 500 °C for 30 min before dipping them in a 0.1 mM Y123 solution in 50/50 (v/v) acetonitrile/t-butanol mixture for 8 hours. The sensitized electrodes were then washed in acetonitrile to remove the loosely bound dye molecule aggregates before the cell assembly. The counter electrode was made by thermally depositing Pt at 410 °C for 20 min from a 5 mM H_2PtCl_6 (Aldrich, Germany) ethanolic solution drop casted on the FTO glass (TEC7, Solaronix, Switzerland). The two electrodes were melt sealed using a 25 µm thick surlyn (Dupont, USA) polymer film. The electrolyte used was a mixture of 200 mM Co^{2+}, 50 mM Co^{3+}, 100 mM $LiClO_4$ and 200 mM tert-butyl pyridine in acetonitrile solvent.[20] The electrolyte was injected by vacuum back filling technique through a hole sand blasted at the side of the counter electrodes.

Photovoltaic Characterization: A 450W xenon lamp (Oriel, USA) was used as solar simulator for photovoltaic (*J–V*) characterizations. The spectral output of the lamp was filtered using a Schott K113 Tempax sunlight filter (Präzisions Glas & Optik GmbH, Germany) to reduce the mismatch between the simulated and actual solar spectrum to less than 2%. The *J–V* characteristics of the cells were recorded with a Keithley model 2400 digital source meter (Keithley, USA). The photo-active area of 0.159 cm^2 was defined using a blackened metal mask. Incident photon-to-current conversion efficiency measurements were determined using a 300 W xenon light source (ILC Technology, USA). A Gemini-180 double monochromator Jobin Yvon Ltd. (UK) was used to select and increment the wavelength of the radiation impinging on the cells. The monochromatic incident light was passed through a chopper running at 1 Hz frequency and the on/off ratio was measured by an operational amplifier. This was superimposed on a white light bias corresponding to 5 mW/cm^2 intensity. The electron transport in the mesoporous film was measured by transient photocurrent decay measurements. The white light was generated by an array of LEDs while a pulsed red light (0.05 s square pulse width) was controlled by a fast solid-state switch to ascertain rapid sub-millisecond rise of light perturbation. The current rise was recorded on a mac-interfaced Keithley 2602 source meter.

Supporting Information

Supporting Information is available from the Wiley Online Library or from the author.

Acknowledgements

The authors acknowledge the financial contribution from EU FP7 project "ORION" grant agreement number NMP-229036. This publication is partially based on work supported by the Center for Advanced Molecular Photovoltaics (Award No KUS-C1-015- 21), made by King Abdullah University of Science and Technology (KAUST). A.K.C. is grateful for financial support from the Balzan foundation as part of the 2009 Balzan Prize award to M.G. M.K.N. thanks the World Class University program, Photovoltaic Materials, Department of Material Chemistry, Korea University, Chungnam, 339-700, Korea, funded by the Ministry of Education, Science and Technology through the National Research Foundation of Korea (No. R31-2008-000-10035-0).

Received: October 10, 2012
Published online: January 15, 2013

[1] A. Fujishima, K. Honda, *Nature* **1972**, *238*, 37.
[2] B. O'Regan, M. Grätzel, *Nature* **1991**, *353*, 737.
[3] U. Bach, D. Lupo, P. Comte, J. E. Moser, F. Weissortel, J. Salbeck, H. Spreitzer, M. Grätzel, *Nature* **1998**, *395*, 583.
[4] A. Yella, H.-W. Lee, H. N. Tsao, C. Yi, A. K. Chandiran, M. K. Nazeeruddin, E. W.-G. Diau, C.-Y. Yeh, S. M. Zakeeruddin, M. Grätzel, *Science* **2011**, *334*, 629.
[5] M. Grätzel, *Nature* **2001**, *414*, 338.
[6] P. V. Kamat, *J. Phys. Chem. C* **2008**, *112*, 18737.
[7] J. Y. Kim, K. Lee, N. E. Coates, D. Moses, T.-Q. Nguyen, M. Dante, A. J. Heeger, *Science* **2007**, *317*, 222.
[8] S. U. M. Khan, M. Al-Shahry, W. B. Ingler, *Science* **2002**, *297*, 2243.
[9] U. Diebold, *Surf. Sci. Rep.* **2003**, *48*, 53.
[10] A. Hagfeldt, G. Boschloo, L. Sun, L. Kloo, H. Pettersson, *Chem. Rev.* **2010**, *110*, 6595.
[11] C. J. Barbé, F. Arendse, P. Comte, M. Jirousek, F. Lenzmann, V. Shklover, M. Grätzel, *J. Am. Ceram. Soc.* **1997**, *80*, 3157.
[12] G. K. Mor, K. Shankar, M. Paulose, O. K. Varghese, C. A. Grimes, *Nano Lett.* **2005**, *6*, 215.
[13] M. Adachi, Y. Murata, J. Takao, J. Jiu, M. Sakamoto, F. Wang, *J. Am. Chem. Soc.* **2004**, *126*, 14943.
[14] F. Sauvage, F. Di Fonzo, A. Li Bassi, C. S. Casari, V. Russo, G. Divitini, C. Ducati, C. E. Bottani, P. Comte, M. Graetzel, *Nano Lett.* **2010**, *10*, 2562.
[15] S. M. George, *Chem. Rev.* **2009**, *110*, 111.
[16] M. Leskelä, M. Ritala, *Thin Solid Films* **2002**, *409*, 138.
[17] S. Nakade, M. Matsuda, S. Kambe, Y. Saito, T. Kitamura, T. Sakata, Y. Wada, H. Mori, S. Yanagida, *J. Phys. Chem. B* **2002**, *106*, 10004.
[18] T. W. Hamann, A. B. F. Martinson, J. W. Elam, M. J. Pellin, J. T. Hupp, *J. Phys. Chem. C* **2008**, *112*, 10303.
[19] L. M. Peter, *Phys. Chem. Chem. Phys.* **2007**, *9*, 2630.
[20] A. K. Chandiran, N. Tetreault, R. Humphry-Baker, F. Kessler, E. Baranoff, C. Yi, M. K. Nazeeruddin, M. Grätzel, *Nano Lett.* **2012**, *12*, 3941.

[21] S. M. Feldt, E. A. Gibson, E. Gabrielsson, L. Sun, G. Boschloo, A. Hagfeldt, *J. Am. Chem. Soc.* **2010**, *132*, 16714.
[22] J. J. Nelson, T. J. Amick, C. M. Elliott, *J. Phys. Chem. C* **2008**, *112*, 18255.
[23] A. K. Chandiran, F. Sauvage, M. Casas-Cabanas, P. Comte, S. M. Zakeeruddin, M. Graetzel, *J. Phys. Chem. C* **2010**, *114*, 15849.
[24] A. K. Chandiran, F. Sauvage, L. Etgar, M. Graetzel, *J. Phys. Chem. C* **2011**, *115*, 9232.
[25] S. O. Saied, J. L. Sullivan, T. Choudhury, C. G. Pearce, *Vacuum* **1988**, *38*, 917.
[26] R. Sanjines, H. Tang, H. Berger, F. Gozzo, G. Margaritondo, F. Levy, *J. Appl. Phys.* **1994**, *75*, 2945.
[27] B. O'Regan, L. Xiaoe, T. Ghaddar, *Energy Environ. Sci.* **2012**, *5*, 7203.
[28] S. Wendt, P. T. Sprunger, E. Lira, G. K. H. Madsen, Z. Li, J. Ã. Hansen, J. Matthiesen, A. Blekinge-Rasmussen, E. Laegsgaard, B. R. Hammer, F. Besenbacher, *Science* **2008**, *320*, 1755.
[29] B. C. O'Regan, J. R. Durrant, P. M. Sommeling, N. J. Bakker, *J. Phys. Chem. C* **2007**, *111*, 14001.
[30] H. N. Tsao, C. Yi, T. Moehl, J.-H. Yum, S. M. Zakeeruddin, M. K. Nazeeruddin, M. Grätzel, *ChemSusChem.* **2011**, *4*, 591.